Numerical simulations of the pseudoelastic effect in CuZnAl shape-memory single crystals considering two successive martensitic transitions

2016 Smart Mater. Struct. 25 025013

(http://iopscience.iop.org/0964-1726/25/2/025013)

IOP Publishing Smart Materials and Structures
Smart Mater. Struct. 25 (2016) 025013 (11pp) doi:10.1088/0964-1726/25/2/025013

Numerical simulations of the pseudoelastic effect in CuZnAl shape-memory single crystals considering two successive martensitic transitions

F de Castro Bubani[1,6], F Lovey[2,3], M Sade[2,3,4] and P Cetlin[5]

[1] Universidade Federal de Minas Gerais, Department of Metallurgical and Materials Engineering, Av. Antonio Carlos 6627, 31270-901 Belo Horizonte, Minas Gerais, Brazil
[2] Centro Atómico Bariloche (CNEA), Av. E. Bustillo km. 9, 5 (8400) S.C. de Bariloche, Argentina
[3] Instituto Balseiro, Universidad Nacional de Cuyo, Av. E. Bustillo km. 9, 5 (8400) S.C. de Bariloche, Argentina
[4] CONICET, Argentina, Av. Rivadavia 1917 (C1033AAJ), Buenos Aires, Argentina
[5] Universidade Federal de Minas Gerais, Department of Mechanical Engineering, Av. Antonio Carlos 6627, 31270-901 Belo Horizonte, Minas Gerais, Brazil

E-mail: franco@cab.cnea.gov.ar

Received 31 August 2015, revised 16 November 2015
Accepted for publication 9 December 2015
Published 21 January 2016

Abstract

Shape memory alloys (SMAs) with double martensitic transitions are potential candidates for highly effective, nonstandard mechanical damping systems. This paper presents a numerical model that can be used to simulate pseudoelasticity in systems with two successive martensitic transformations, such as adequately oriented CuZnAl, CuAlNi and CuAlBe single crystals. The model is based on stress versus strain data obtained from the tensile test of a CuZnAl single crystal and is able to simulate the mechanical damping of SMAs with two successive martensitic transitions. The numerical model has been implemented as an algorithm and used to assess the mechanical damping capacity of a system based on CuZnAl SMA single crystals, considering the complete β-18R–6R cycle. A numerical model with a single degree of freedom is used and the behavior of the SMA-based damper is analyzed both under free and forced oscillation conditions. The results obtained indicate that the alloy studied is a very effective mechanical damper.

Keywords: numerical simulations, shape-memory effect, martensitic transformations, pseudoelasticity, CuZnAl, single crystals

(Some figures may appear in colour only in the online journal)

Introduction

Depending on the specific chemical composition, many alloys as, for example, NiTi, Cu-base and Fe-base shape-memory alloys (SMAs), in a certain temperature range above the martensite start (M_s) temperature, show pseudoelastic behavior [1–10]. These alloys undergo a stress-induced martensitic transition when the load is applied and, when the load is removed, they retransform to the original austenitic phase. The transformation stress is usually higher than the retransformation stress, which leads to hysteresis in the load curve. The hysteresis associated to the pseudoelastic behavior in SMAs can be used in mechanical damping devices, as a certain amount of energy is dissipated in each load cycle [11]. Several systems show a second phase transition if the stress induced martensite is strained further. As an example, we can

[6] Author to whom any correspondence should be addressed.

mention the transitions reported in NiFeGa single crystals [12, 13]. Other known examples have been reported in Cu-base alloys. Some Cu-base SMA single crystals, depending on their chemical composition and crystallographic orientation of the tensile axis, show two successive martensitic transformations induced by tension: β-18R and 18R–6R [7, 14–16]. When the load is removed, the alloy retransforms back to its original austenitic structure (β).

Moreover, because of the fact that the hysteresis associated with the 18R–6R transformation is very large, this transition is especially interesting for potential damping devices, as the energy dissipated per cycle is many times greater than in the β-18R transition. The double sequential martensitic transition can be observed in CuZnAl, CuAlNi [17] and CuAlBe [18, 19] for tensile axes close to the [001] crystallographic orientation. As a general rule, temperature and thermal effects play significant roles during martensitic phase transformations, as transformation stresses are usually temperature dependent. However, the 18R–6R martensitic transformation shows a well-defined plateau during the transformation and the critical stress to induce the 6R phase shows a very small, negative dependence on temperature [7, 20]. This means that if the temperature increases several degrees K, the 18R–6R transformation stress will decrease only a few MPa. The exact value of the stress drop can be predicted from the Clausius–Clapeyron relationship, which relates changes in temperature (ΔT) to changes in transformation stress ($\Delta\sigma$) for a given phase transition [7, 20]. Moreover, different types of mechanical behavior can be obtained according to the test temperature, since the Clausius–Clapeyron relationship corresponding to the first martensitic transition (β-18R) exhibits a stronger dependence of critical stresses on test temperature than the 18R to 6R transition.

Compared to NiTi, the 18R–6R transition in CuZnAl provides an interesting advantage in applications where significant temperature variations are expected, e.g., outdoors in temperate climates, because martensitic transition stresses in NiTi are very sensitive to temperature [3]. Because of this fact, the mechanical behavior of damping devices based on NiTi should be more sensitive to seasonal or even night/day temperature variations. Moreover, the enthalpy difference between phases in NiTi leads to significant heating or cooling of the material during mechanically-induced transitions, especially at high transformation speeds which, in turn, modifies the mechanical behavior of the damping device.

A brief description of the dynamics of one degree-of-freedom mass–spring systems, with and without SMA damping, is provided below. Additional details can be found in [21].

The differential equation that describes a linear, one degree-of-freedom system submitted to an external harmonic excitation can be readily obtained from Newton's second law by considering all forces involved in the problem:

$$m\ddot{x} + c\dot{x} + kx = F_0 \cdot \cos(\omega t), \tag{1}$$

where m is the equivalent mass, c is the viscous damping, k is the elastic constant, F_0 is the amplitude of the external force, ω is the angular frequency of the external force and t is time. The steady-state regimen of the system, at a given angular frequency ω, is the particular solution of equation (1):

$$x(t) = X.\ \cos(\omega t - \varphi), \tag{2}$$

where x is the position, φ is the phase angle and X is the amplitude of the response, given by:

$$X = \frac{\delta_{st}}{\sqrt{(1 - r^2)^2 + (2\zeta r)^2}}, \tag{3}$$

where δ_{st} is the static deflection of the spring, given by:

$$\delta_{st} = \frac{F_0}{k}, \tag{4}$$

r is the ratio between the external excitation frequency ω and the natural frequency ω_n:

$$r = \frac{\omega}{\omega_n}. \tag{5}$$

The natural frequency ω_n is given by:

$$\omega_n = \sqrt{\frac{k}{m}}\ . \tag{6}$$

ζ is the damping ratio, given by:

$$\zeta = \frac{c}{2\sqrt{mk}}. \tag{7}$$

According to equations (1)–(7), a linear, one degree-of-freedom system responds to an external harmonic excitation by oscillating at exactly the same frequency of the excitation. However, the amplitude of the response and the phase angle depend on several factors, namely: the amplitude of the external force, the ratio between the frequency of the external force and the natural frequency of the system and also the viscous damping present.

It must be emphasized that equations (2)–(7) are only applicable to linear mass–spring systems submitted to harmonic excitations, not to SMA-based systems. According to the principle of superposition of forces, it is possible to describe the behavior of mass–spring systems with SMA damping by adding the force generated by the SMA to equation (1). We obtain:

$$m\ddot{x} + c\dot{x} + kx = F_0 \cdot \cos(\omega t) + F_{SMA}, \tag{8}$$

where F_{SMA} is a generalized function that returns the force generated by the SMA damping system. The arguments of F_{SMA} depend on the specific model and parameters such as temperature and the accumulated number of cycles may be considered in complex simulations. In this paper, F_{SMA} is a function of the martensitic transformation stresses, the geometry of the SMA single crystals, the elasticity of the system, x, $\dot{x}$ and the SMA stress in the previous integration step, as described in the Methods section below.

The presence of SMA damping makes the system nonlinear and, to the extent of the authors' knowledge, no simple, algebraic solutions to systems with damping based on SMAs with double martensitic transformations are available. However, numerical solutions to equation (8) can be readily obtained, once F_{SMA} is defined. The approach adopted in this

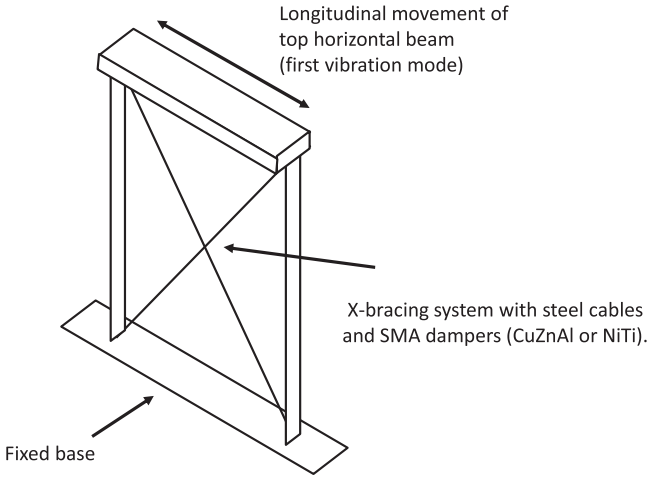

Figure 1. The porch that was used as a base for the simulations. X-bracing is done with steel cables. A SMA single crystal is placed along each cable so that whenever relative movement between the top and the base of the porch occurs, one of the cables is submitted to tension and the other is free from loads. Adapted from [28] with modifications.

work to calculate F_{SMA} and the numerical method used to obtain approximate solutions is described in the methods section.

Several approaches have been considered to simulate the mechanical behavior associated to pseudoelasticity where only one transformation is taken into account, i.e., from austenite to martensite, especially in NiTi alloys. As an example, Torra *et al* [11] present two different models to reproduce the behavior of NiTi in damping devices: a bilinear model, which considers that, during the martensitic transition, both transformation and retransformation stresses depend linearly on strain, and a cubic model, which considers that, during the martensitic transition, transformation and retransformation stresses are cubic functions of strain. The bilinear model is simpler, but its accuracy is limited. The cubic model, on the other hand, is more accurate and more complex. Both models are able to describe partial transformation loops.

Other models to simulate NiTi SMAs were presented in [22, 23]. Some models go further and consider crystallographic orientation and martensite variants, such as in [24, 25]. Rao *et al* presented a model to simulate torsion in SMA wires [26]. Li *et al* presented a model to simulate ferromagnetic SMAs [27]. However, to the extent of the authors' knowledge, no model with two sequential martensitic transitions has been proposed to date. The mechanical behavior of these alloys when two sequential transitions are taken into account is complex and there is no information in the literature regarding numerical simulations of these systems.

In this paper, a numerical algorithm that is able to simulate the pseudoelasticity associated with the austenite to martensite transition and a subsequent martensite to martensite transformation is presented. The model considers that all martensitic transformations and retransformations occur at constant stresses, and also considers the linear elastic deformation of the austenite and the 18R martensite. The model is able to reproduce partial loops in such a way that the load can be reversed at any point of the stress–strain curve.

The model was applied to a mass–spring system with one degree of freedom so as to assess the damping capacity of the SMA with two sequential martensitic transitions in a harmonic oscillator. The idea is to simulate the first vibration mode of the porch with x-bracing (figure 1), which corresponds to longitudinal oscillations of the upper part of the porch. The porch was originally developed by Soul [28] to test NiTi SMA wires. Some modifications were implemented so that two CuZnAl SMA single crystals with sequential martensitic transitions are placed in the bracers, i.e., one crystal for each diagonal bracer. The model proposed is a first approximation of the problem and the authors hope that it will encourage the development of more complex algorithms that take into consideration variables such as thermal effects and differential martensitic stabilization.

Methods

Even though data is available in the literature concerning the sequential transformations in CuZnAl single crystals [7, 19], a specific test has been performed to obtain the required data for the numerical model. A Cu—14.78 at%Zn—16.61 at%Al single crystal with electronic concentration $e/a = 1.48$ and tensile axis [1, 2, 20] was manufactured in the Metals Physics Division of Centro Atómico Bariloche. A tension test sample was obtained from the single crystal by mechanical turning, and was then submitted to the following thermal treatment: 30 min at 1173 K followed by air cooling to 523 K and quenching in water at 278 K. This thermal treatment has been reported in the literature and is known to introduce a uniform distribution of nanoprecipitates [29]. The effect of these precipitates on the β-18R phase transformation was analyzed in several papers [30–32] and more recently it has been shown that they harden the alloy, making it possible to obtain the 6R martensite without plastic deformation [19].

Finally, the sample was submitted to a tensile test at 303 K on an Instron 5567 machine equipped with a temperature chamber. The crosshead speed was kept constant at 0.3 mm min^{-1} and strain was measured by an Instron 2620-602 extensometer. The experimental stress versus strain curve obtained is shown in figure 2. Both martensitic transformations (β-18R and 18R–6R) are clearly seen in the graph, and critical stress values can be obtained. When both martensitic transformations are considered, the total recoverable deformation of the alloy can be over 20% (figure 2).

The data obtained from the tension test was used to create a preliminary numerical model of the mechanical behavior of the alloy. The model considers the sequential martensitic transformations of the alloy and the combined elasticity of the SMA and the mechanical system to which it is connected. The numerical model is, thus, able to approximate the stress versus strain curve shown in figure 2. As this is a preliminary model, stabilization of martensite and thermal effects are not taken into account, i.e., martensitic transformation and retransformation stresses are considered constant and plastic

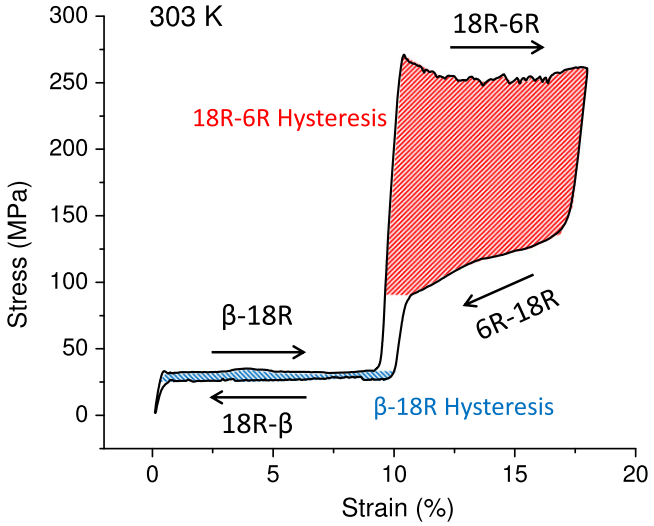

Figure 2. Tensile stress versus strain curve of a (Cu—14.78 at%Zn—16.61 at%Al) single crystal, with two sequential martensitic transitions (β-18R and 18R–6R, with their respective retransformations). The approximate hysteresis of each transformation is indicated by the shaded areas in the curve.

deformation and martensite stabilization are disregarded. It is important to emphasize that, in the present work, there are two martensitic transitions involved and such effects are significantly more complex than in SMAs that have only one martensitic transition. It is also important to mention that some phenomena related to the double martensitic transformation are not completely understood. However, as the Clausius–Clapeyron coefficient of the 18R–6R transformation is very small [5, 7], the critical stress to induce 6R has a very weak dependence on temperature. Thus, it is reasonable to disregard thermal effects on the 18R–6R transition, as a first approach. This is by no means a general rule and care must be taken if other transitions are considered.

The numerical model was implemented in the programming language Python 3.4, in a damped mass–spring system with one degree of freedom. The algorithm calculates the instant value of the force generated by the SMA (represented by F_{SMA}, in equation (8)), considering that the SMA may have two sequential martensitic transitions, and then solves equation (8) numerically, for every integration step. The mass, elasticity and viscous damping of the system were adjusted to match the behavior of the prototype porch developed by Soul, with small modifications [28]. A value of 58 000 N m^{-1} for the equivalent stiffness coefficient k and an equivalent mass M of 30 kg were considered, which leads to a fundamental frequency ω of approximately 7 Hz.

The preliminary numerical model presented in this work is purely mechanical and is able to approximate the behavior of alloys with two sequential martensitic transitions (β-18R and 18R–6R, in CuZnAl SMA single crystals). Alloys with one martensitic transition, e.g., NiTi, can also be simulated. The model considers that transition stresses are kept constant. The information related to the porch that needs to be provided to the model before the simulation can be run is the equivalent elasticity of the porch with the bracing system, the equivalent mass and viscous damping of the system. Moreover, the cross-section area and length of the SMA must also be provided, so that the stress versus strain curve of the SMA can be converted to force versus displacement data. Four transition stress values must be provided as inputs for the simulations with CuZnAl: β-18R, 18R–6R, 6R–18R and 18R-β (the first two correspond to martensitic transformations and the last two correspond to martensitic retransformations).

As the pseudoelastic effect is characterized by its stress hysteresis, it is not possible to determine the stress value considering only the displacement, i.e., for a given displacement value, the SMA may be submitted to different stress values depending on whether the load is being applied or removed. In the first case, the SMA is submitted to the corresponding martensitic transformation stress and, in the second case, to the retransformation stress. Other stress values are also possible, because of the elasticity of the system; this is discussed below together with partial cycles. Therefore, the model also needs the first derivative of the displacement, i.e., velocity, at every integration step, to determine if the SMA is undergoing martensitic transformation or retransformation, and calculate the correct stress value.

The velocity at which martensitic transitions occur may have an effect on transition stresses because of thermal effects related to entropy differences between phases. The magnitude of this effect depends on the specific alloy and the martensitic transition considered. However, as this is a preliminary model, thermal effects are not considered, so only the sign of the velocity is taken into account.

The last variable needed by the model is the stress calculated in the previous integration step. This value, combined with the total elasticity of the system, is used to simulate partial cycles. In every integration step, the model calculates the difference in displacement between the current and the previous integration steps. The maximum stress variation is then calculated according to Hooke's law, by considering the total elasticity of the system and the difference in displacement between steps. This value is used to limit stress variations between steps in the model, and the final result is that any kind of partial cycles can be reproduced by the model, as stress variations are smoothed according to the total elasticity of the system. For example, if the movement is inverted at any time during the 18R–6R transition, the stress will decrease linearly, with a slope that corresponds precisely to the combined elasticity of the system, until the 6R–18R retransformation stress is reached. The same behavior is observed if the direction is reversed during the β-18R transformation but, in this case, the stress will decrease linearly, with the same slope, until the 18R-β stress is reached. This purely mechanical approach is relatively simple, yet very effective and provides a reasonable approximation of experimental data according to the elasticity of the system. Other variables, such as thermal effects, martensite stabilization and stress variations during the martensitic transitions may be included in future models.

The integration method used was proposed by Newmark [33]. It is a numerical method to solve structural dynamics problems, and it may be applied to any structure with a finite

number of degrees of freedom, in the elastic or plastic range, submitted to any kind of dynamic loads. In the following equations, x is the position, $\dot{x}$ the velocity, $\ddot{x}$ the acceleration, and the underscores indicate the number of the integration step. Δt is the time interval between steps $(n + 1)$ and n. The velocity in step $(n + 1)$ can be calculated by:

$$\dot{x}_{n+1} = \dot{x}_n + \Delta t.\ \ddot{x}_\gamma, \tag{9}$$

where

$$\ddot{x}_\gamma = (1 - \gamma)\ddot{x}_n + \gamma.\ \ddot{x}_{n+1} \qquad 0 \leqslant \gamma \leqslant 1, \tag{10}$$

where γ is a non-dimensional parameter introduced to calculate a weighted average of the values of $\ddot{x}_n$ and $\ddot{x}_{n+1}$ to calculate $\dot{x}_{n+1}$.

Thus

$$\dot{x}_{n+1} = \dot{x}_n + (1 - \gamma)\Delta t.\ \ddot{x}_n + \gamma\Delta t.\ \ddot{x}_{n+1}. \tag{11}$$

The value of $\ddot{x}_{n+1}$, i.e., the acceleration at the end of the integration step, must be known before the equation above can be calculated, except if $\gamma = 0$. Usually, $\ddot{x}_{n+1}$ is not known in advance. It is still possible to use $\gamma = 0$ to avoid this problem, but this would introduce other difficulties: Newmark demonstrates that damping is added to the system as an undesired effect of the numerical algorithm and that this damping is proportional to $(\gamma - 0.5)$ [33]. Therefore, using $\gamma = 0$ would result in negative damping, i.e., the system would be self-excited and energy would be introduced. This effect has no physical meaning and is merely a numerical artifact caused by a poor choice of parameters. Newmark suggests using $\gamma = 0.5$ so that this unwanted effect is completely eliminated. If damping forces are present in the system, viscous or otherwise, the total damping force should be calculated and added to the other forces acting on the system, at each integration step. This is the approach adopted in our model.

The position also depends on the acceleration, both in the beginning and at the end of the integration step. A new non-dimensional parameter, β, is introduced in order to calculate a weighted average of $\ddot{x}_n$ and $\ddot{x}_{n+1}$ in the calculation of x_{n+1}. With $\gamma = 0.5$, the position at the end of the integration step is:

$$x_{n+1} = x_n + \Delta t.\ \dot{x}_n + 0.5\Delta t^2.\ \ddot{x}_\beta, \tag{12}$$

where

$$\ddot{x}_\beta = (1-2\beta)\ddot{x}_n + 2\beta.\ \ddot{x}_{n+1} \qquad 0 \leqslant 2\beta \leqslant 1. \tag{13}$$

With $\gamma = 0.5$, the equations of velocity and position become, respectively:

$$\dot{x}_{n+1} = \dot{x}_n + 0.5\Delta t.\ (\ddot{x}_n + \ddot{x}_{n+1}), \tag{14}$$

$$x_{n+1} = x_n + \Delta t.\ \dot{x}_n + (0.5 - \beta).\ \Delta t^2\ddot{x}_n + \beta\Delta t^2.\ \ddot{x}_{n+1}. \tag{15}$$

The value of β affects the stability, the convergence and the accuracy of the method [33]. The value that is normally adopted is $\beta = 0.25$, in which case the method is called the average acceleration method:

$$x_{n+1} = x_n + \Delta t.\ \dot{x}_n + 0.25.\Delta t^2.\ (\ddot{x}_n + \ddot{x}_{n+1}), \tag{16}$$

$$\dot{x}_{n+1} = \dot{x}_n + 0.5.\Delta t.\ (\ddot{x}_n + \ddot{x}_{n+1}). \tag{17}$$

Still, the acceleration at the end of the integration step $\ddot{x}_{n+1}$ must be known in advance, so that equations (16) and (17) can be calculated. As it is not usually possible to calculate this value in advance, an estimation must be made and the method becomes iterative: calculations are first carried out with an estimated value of $\ddot{x}_{n+1}$. A new value of $\ddot{x}_{n+1}$ is obtained and compared to the originally estimated value. After that, calculations are repeated, now using the calculated value of $\ddot{x}_{n+1}$ as the estimation, and so on, until the difference between the estimated and calculated values of $\ddot{x}_{n+1}$ is equal to or smaller than the convergence criterion adopted.

The model presented in this paper uses an iterative implementation of the Newmark method, with $\gamma = 0.5$ and $\beta = 0.25$. In our model, convergence is achieved when the difference between the estimated and calculated values of x_{n+1} is smaller than or equal to the precision of the double-precision floating-point number format used in the algorithm. As the convergence criterion adopted is very strict, the accuracy of the results obtained is maximized. However, the number of iterations per integration step increases, which also increases the total time required for each simulation. Longer simulation times were partially compensated by advanced algorithm optimization techniques.

The integration step in all simulations was set to 10^{-4} s. This value is more than one order of magnitude below the value at which stability and convergence issues were observed at the frequencies simulated, with SMA damping. To validate our results, simulations were run with even smaller integration steps and the results obtained were identical.

The program allows us to compare different situations, with or without external excitation. The damping capacity of the system with SMA was analyzed and the results of the system with and without SMA damping were compared. The numeric model with one degree of freedom was validated by an analytical comparison of the results obtained.

The model can be understood as a multi variable function that approximates the mechanical behavior of the SMA. The output is a force value, which depends on the predefined boundary conditions, i.e., the geometry of the SMA and the equivalent elasticity of the system, and the instantaneous values of displacement and velocity. The force generated by the SMA is calculated at each iteration: it is applied to the mass and the resulting force is used to calculate the acceleration of the system. After numerical integration to calculate the velocity and position at the end of the step, another iteration takes place: the force generated by the SMA is recalculated and applied to the mass, and the whole process is repeated, until convergence is achieved at each step. A diagram of the simulation is shown in figure 3.

The second martensitic transformation in CuZnAl (18R–6R) has only been observed in tension, so we need two SMA elements to create a one degree-of-freedom damping device that applies a force that is symmetrical regarding positive and negative displacements. The device must be built in such a way that each SMA damping element only works for half cycle. At the equilibrium position, corresponding to displacement $x = 0$, no loads are applied to the SMA elements.

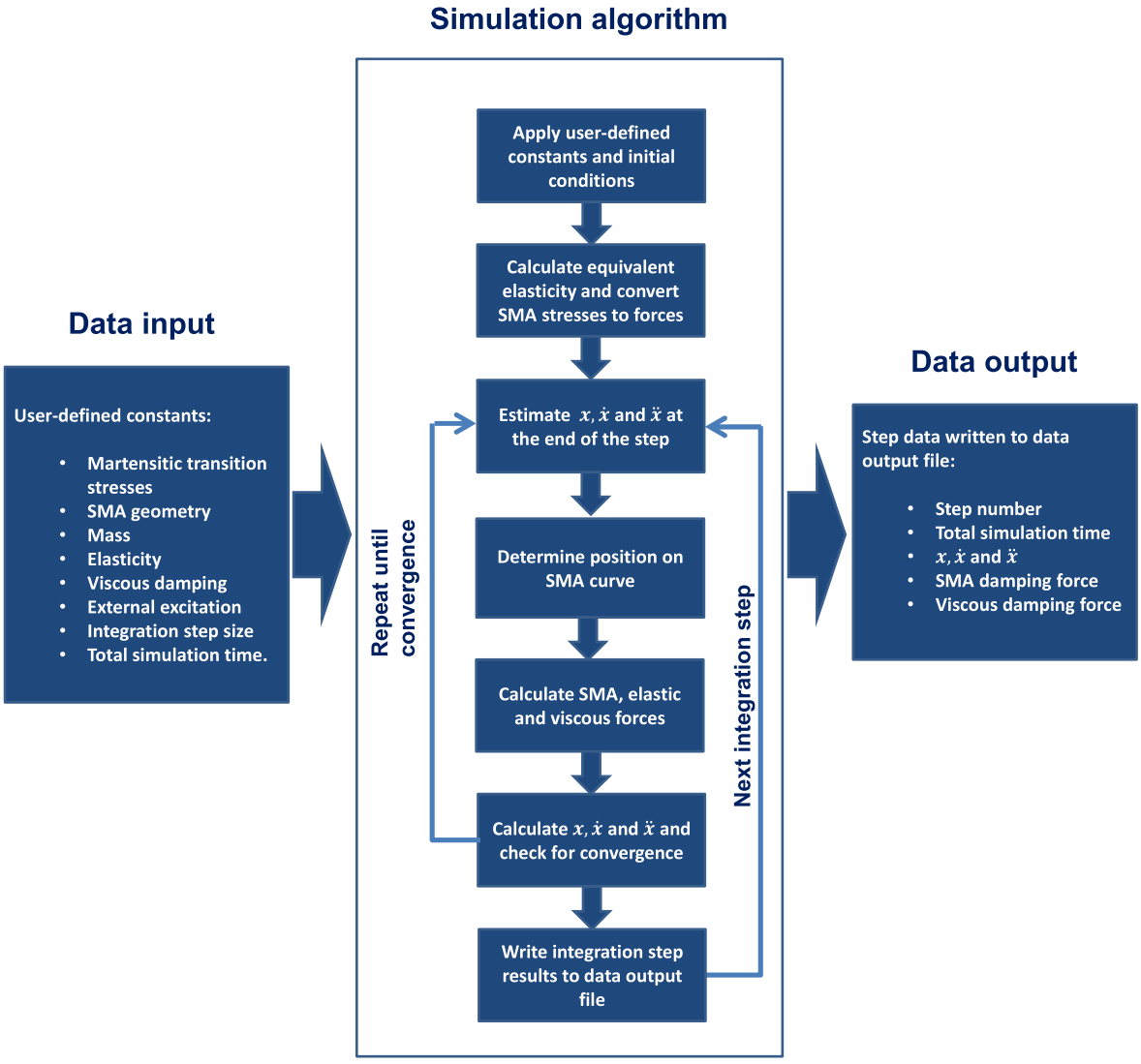

Figure 3. A simplified diagram of the simulation algorithm.

For $x > 0$, one SMA element is under tension while the other is free from external loads. For $x < 0$, the element that was previously under tension (for $x > 0$) is now free from external loads, while the other element, that was previously free from external loads, is now under tension. So, when one SMA damping element is under tension, no external load is applied to the other, and vice versa. The final result is a damping device that is not linear, but which is capable of applying a symmetrical force for positive and negative displacements.

The behavior of the SMA was modeled considering that each element is a single crystal with 0.02 m length and 0.0025 m diameter, unless specifically mentioned. In the model, the martensitic transformation and retransformation stresses are constant and approximate the real behavior of the material with precipitates, described above. The values of the transformation stresses are: $\sigma^{\beta-18R} = 35$ MPa, $\sigma^{18R-6R} = 250$ MPa, $\sigma^{18R-\beta} = 25$ MPa, σ^{6R-18R}=115 MPa (figure 4) (the corresponding martensitic transition is shown in superscript). These critical transformation stresses depend

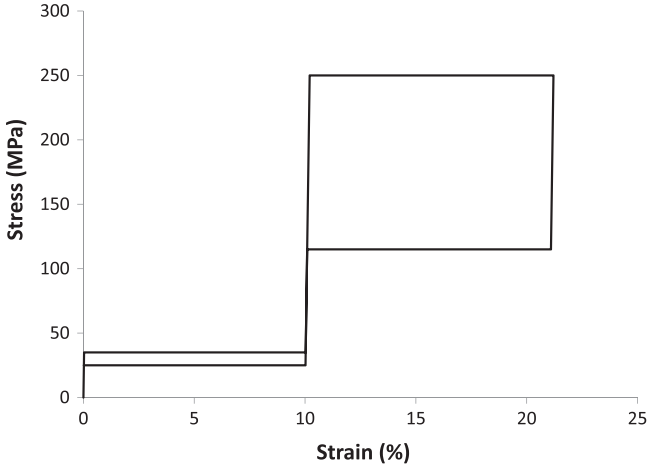

Figure 4. Simulated stress versus strain behavior of each SMA single crystal. The model is also able to simulate partial loops.

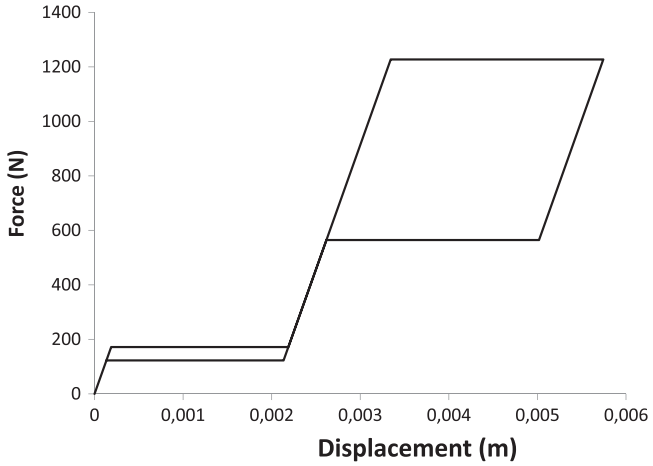

Figure 5. Simulated force versus displacement curve (absolute values), considering the geometry and the combined elasticity of the whole system. The elasticity is also considered in partial loops. Force and displacement are used in this figure to facilitate the analysis in further simulations of the mechanical behavior of the experimental system.

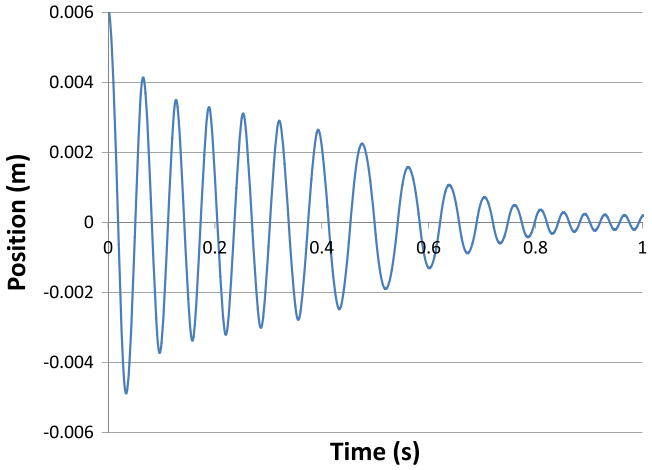

Figure 6. Simulation of the dynamic behavior of the system with damping provided by the complete β-18R–6R cycle. The damping observed in the first cycles is due to the 18R–6R transformation, which has a very high hysteresis of approx. 135 MPa. The hysteresis of the β-18R transformation is approximately one order of magnitude smaller.

on the temperature and on the crystallographic orientation of the tensile axis. It is possible, thus, to simulate the behavior of the alloy at different temperatures by changing the martensitic transition tensions, according to the Clausius–Clapeyron relations available in the literature [5, 7], after corrections by the Schmid factor. Moreover, the model considers the elasticity of the system as follows: each sample is attached to a mechanical system that has the equivalent elasticity of a 0.7 m long carbon steel wire with 0.002 m diameter, which approximates the x-bracing system of the porch. The simulated stress versus strain behavior of a SMA single crystal is shown in figure 4.

The elastic strain of the SMA single crystal is very small compared with the summed pseudoelastic strain of both martensitic transitions. However, to better approximate the physical behavior of SMAs in damping applications, one must consider the elasticity of the mechanical system to which the SMA single crystals are attached, which is shown in figure 5. The combined elasticity of the whole system simulated is significant when compared to the pseudoelastic strain of the SMA. Please note that the elasticity depends heavily on the specific mechanical system used, so the curve shown in figure 5 only represents the porch modeled in this work and is not representative of other systems.

Results

The model was used to simulate free and forced oscillations. The first simulation corresponded to free oscillations after an initial displacement of 6×10^{-3} m (figure 6). In this simulation, the damping provided by the SMA is considered, and also the small viscous damping inherent to the porch was included. The equivalent viscous damping coefficient c used in free simulations is $c = 9.3\,\mathrm{N\,s\,m^{-1}}$, which is very small compared to the damping capacity of the SMA used. Both β-18R and 18R–6R martensitic transitions were considered in these simulations. In the first cycle, the SMA is submitted to β-18R–6R sequential transformations and the energy dissipated is very large. In the second cycle, only a small fraction of the material transforms to 6R martensite. From the third cycle on, the amplitude in not sufficient to induce the high hysteresis 18R–6R transformation anymore and the dissipation of energy per cycle is significantly reduced (the state of the SMA single crystals during the simulation can be easily verified comparing the position in figure 6 and the simulated force versus displacement curve in figure 5). This behavior is reflected in figure 6, where a significant slope change of the envelope marks the change in the regimen mentioned above (initially, β-18R–6R and then only β-18R). Because of the highly nonlinear characteristics of the SMA damper modeled, the frequency of the system changes during the simulation. At about 0.9 s into the simulation, the amplitude of the oscillations is no longer enough to induce the β-18R transformation, i.e., no martensitic transformation occurs in the SMA single crystals and the only energy absorption present in the model is the very small viscous damping inherent to the porch. At this point, the system keeps oscillating with lower amplitudes, which correspond to the elastic zone of the β phase of the SMA, where the only damping is the one provided by the viscosity of the model. In these conditions, the amplitude decays exponentially towards zero, as an underdamped harmonic oscillator.

The numerical model was then submitted to a frequency sweep, with and without the presence of the SMA dampers. For the frequency sweeps, the viscous damping coefficient was increased to $c = 50\,\mathrm{N\,s\,m^{-1}}$. This is necessary to limit the dynamic response in conditions close to resonance in the model without SMA damping. To make the comparison of the results easier, the same viscous damping coefficient was used in the system with SMA, even though the maximum

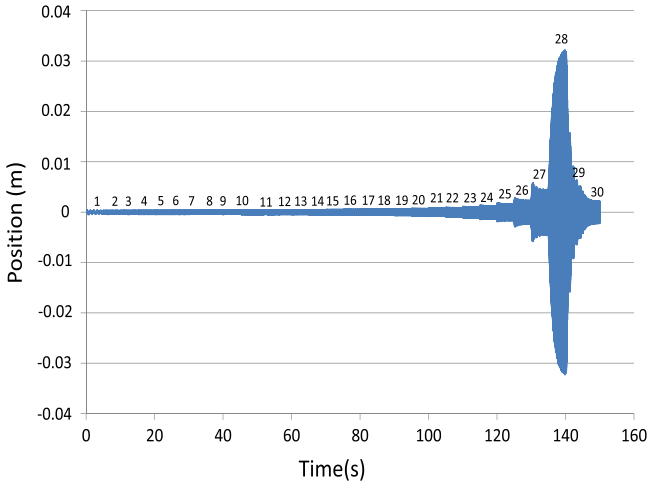

Figure 7. Frequency sweep of the system with steel tensors but without SMA. The numbers over the curve indicate the frequency in Hz. The resonance frequency is increased to 28 Hz.

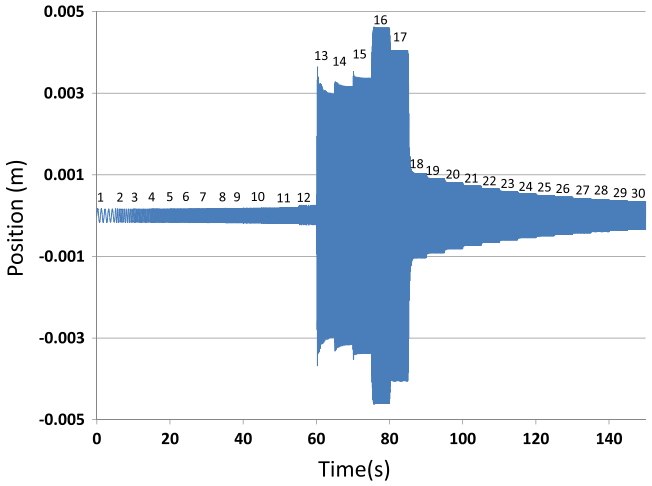

Figure 8. Frequency sweep with SMA damping, with both martensitic transformations (β-18R–6R). The numbers above the curve indicate the frequency in Hz.

oscillation amplitude in these cases is limited by the huge damping provided by the SMA. A frequency sweep from 1 Hz to 30 Hz was done, using steps of 1 Hz. The frequency was kept constant at every step for 5 s. The external excitation used was a sinusoidal acceleration with maximum amplitude of 5 m s^{-2}.

A frequency sweep simulation of the porch without bracing or SMAs was run. As expected, the maximum response corresponds to the fundamental frequency calculated above, approximately 7 Hz, and is limited only by the viscous damping. In order to isolate the SMA damping effect from the increase in the rigidity due to the diagonal tensors, a simulation with the x-bracing but without SMA damping was done (figure 7). The steel cables significantly increase the rigidity of the system and the maximum response frequency is increased to 28 Hz.

The same simulation was repeated with the SMA damper, considering the complete β-18R–6R cycle (figure 8). The dynamic behavior of the system is clearly nonlinear and the maximum dynamic response occurred at 19 Hz. The oscillation amplitude obtained at 7 Hz is very small.

In order to highlight the advantages of the 18R–6R martensitic transformation in CuZnAl SMAs compared to the B2–B19 transition in NiTi SMAs, frequency sweep simulations were done at two different temperatures (271 K and 323 K), for each alloy. In CuZnAl, only the 18R–6R transition was considered, which can be achieved by stabilizing a mechanically-induced 18R single crystal. The martensitic transformation and retransformation stresses of NiTi were taken from [3], considering cycle $n = 30$ at 323 K, and are equal to 520 MPa and 425 MPa, respectively. For the simulation at 271 K, martensitic transformation and retransformation stresses were calculated considering the value of the Clausius–Clapeyron coefficient of the B2–B19 transition in NiTi (6 MPa K^{-1}), and are equal to 208 MPa and 113 MPa, respectively. In the simulations, stress hysteresis is equal to 95 MPa at both temperatures. In order to approximate the

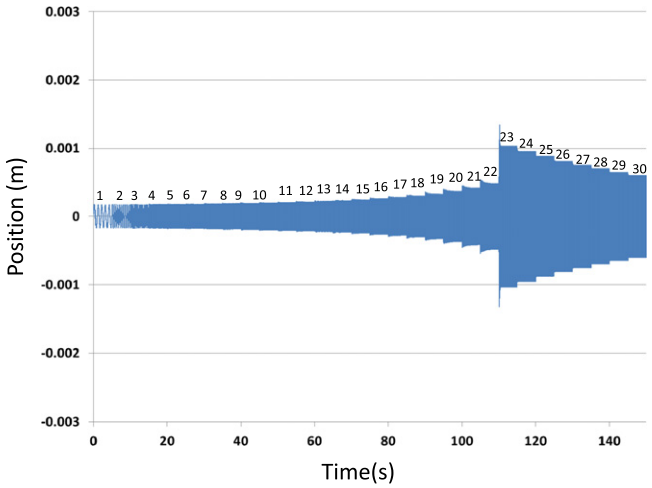

Figure 9. Frequency sweep with NiTi SMA damping. The simulated temperature is 271 K. The numbers above the curve indicate the frequency in Hz.

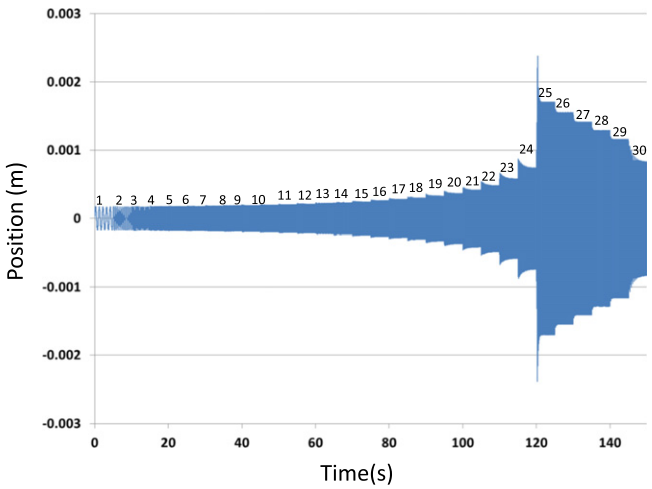

Figure 10. Frequency sweep with NiTi SMA damping. The simulated temperature is 323 K. The numbers above the curve indicate the frequency in Hz.

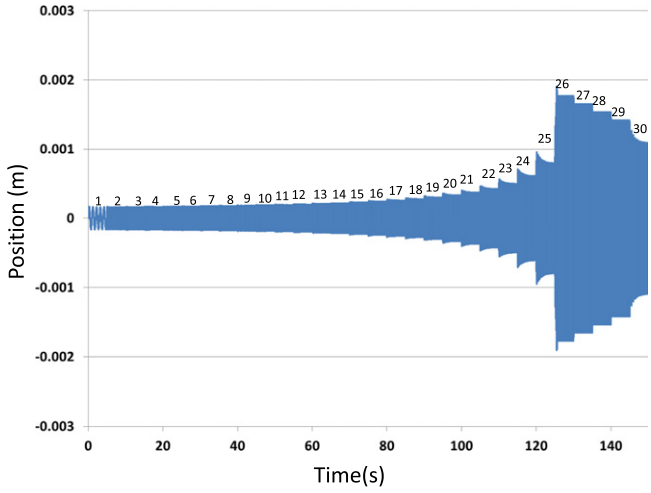

Figure 11. Frequency sweep with CuZnAl SMA damping. Only the 18R–6R transition is considered. The simulated temperature is 323 K. The numbers above the curve indicate the frequency in Hz.

forces generated by the SMA damping elements, the simulations considered that the diameter of the NiTi wires were equal to 1.5 mm. The simulated diameter of CuZnAl single crystals is 2.5 mm.

In NiTi transition stresses at 271 K are approximately 312 MPa smaller than those at 323 K. This difference is significant and is reflected in the dynamic behavior of the system (figures 9 and 10). At 271 K, smaller stresses (and, consequently, smaller displacements) are needed to induce the martensitic transition in NiTi. This means that the damping action of the SMA is active at smaller amplitudes than at 323 K, making it much more effective at 271 K than at 323 K. This effect can be clearly seen comparing the amplitudes in figures 9 and 10 at 25 Hz and above: at 271 K (figure 9), the amplitude is considerably smaller than at 323 K (figure 10). Moreover, the maximum dynamic response at 271 K is observed at 23 Hz, whereas at 323 K the peak response is seen at 25 Hz. These results demonstrate that the behavior of NiTi SMA based mechanical dampers can be significantly affected by temperature variations.

On the other hand, the 18R–6R transition stresses in CuZnAl are only slightly affected by temperature, i.e., the Clausius–Clapeyron coefficient is small (-0.4 MPa K^{-1}). The difference in the simulated frequency sweeps at 271 K and 323 K is small, which is why only the results of the simulation at 323 K are shown (figure 11).

Discussion

In the simulations done for the free oscillations, the SMA introduces significant damping on the system (figure 6). Originally, the amplitude of oscillation is enough to submit the SMA to the complete β-18R–6R cycle. The hysteresis is very large and, consequently, so is the energy dissipation in each cycle. After few oscillations, the amplitude of the system is no longer enough to cycle the SMA through both sequential martensitic transitions. Only the first martensitic transition (β-18R) occurs. The energy dissipation in each cycle is considerably reduced, as the hysteresis of the β-18R transformation is much smaller than the hysteresis of the 18R–6R transformation. Nevertheless, the hysteresis of the SMA damper keeps dissipating the energy of the system, until the amplitude is so small that the SMA is restricted to the elastic phase of the austenite, i.e., no martensitic transitions occur and energy is no longer dissipated by the SMA. If no other damping mechanisms were present, such as viscous damping, the system would keep oscillating with constant amplitude, which could be considered the steady state of the system. However, some viscous damping is considered in our simulations, so the amplitude decreases asymptotically towards zero.

From the results shown in figure 7 (forced oscillations), we can observe that the system with x-bracing but without SMA damping is linear and behaves according to theory: the system behaves linearly and the maximum amplitude at resonance is only limited by the viscous damping. The introduction of diagonal tensors on the porch significantly changes its dynamic behavior because of the increase in the rigidity of the system: the resonance frequency increases and the amplitude of oscillation decreases in all the frequency range analyzed, except at frequencies close to the natural frequency of the system (approximately 28 Hz). Nevertheless, no increase in the dissipation of energy is observed, which clearly happens once the SMA damper is introduced.

The behavior of the system with SMA damping and forced oscillations (figure 8), submitted to a frequency sweep, is different. On the one hand, the presence of SMA damping increases the rigidity of the system, which, in turn, shifts the maximum dynamic response from 7 Hz to higher values. In figure 8, we can observe that the maximum dynamic response of the system occurs at 16 Hz, with an amplitude of, approximately, 4.5×10^{-3} m. The response of the system at 7 Hz is very small. It should be emphasized that the SMA damping presented in this paper is highly nonlinear, so the results obtained from the frequency sweep simulation are specific to the boundary conditions considered and should not be extrapolated. For instance, the frequency where maximum dynamic response is observed depends on the amplitude of the excitation.

Compared to the porch with tensors but without SMA (figure 7), we can observe that the maximum amplitude of oscillation of the porch with SMA (figure 8) corresponds to only 15% of the maximum amplitude of the porch only with steel tensors. This difference is very large and demonstrates the beneficial effect of SMA damping. The increase in the rigidity of the system can be beneficial in seismic resistant structures because it limits the amplitude of oscillation and increases the frequencies of their corresponding vibration modes. Nevertheless, the introduction of the SMA damper, besides increasing the rigidity of the system, adds significant hysteretic damping associated with the mechanically induced martensitic transitions. With SMA, the maximum amplitude of oscillation is considerably smaller than without SMA and nonlinear effects appear on the system.

Compared to NiTi, 18R–6R transition stresses in CuZnAl are much more stable regarding temperature variations. This fact can be used to produce damping devices whose mechanical behavior is more predictable, especially in outdoors applications.

The apparently better damping capacity of NiTi at 271 K (figure 9), compared with CuZnAl (figure 11) is due to smaller NiTi martensitic transformation stresses at this temperature, combined with a smaller diameter of the NiTi SMA. The result is that, under these conditions, significantly smaller forces are required to induce the martensitic transformation in NiTi than in CuZnAl. As the force applied to the SMA is related to the position of the system, the amplitude of movement of the mass–spring system must be sufficiently high for the SMA to reach the martensitic transformation stress, otherwise the pseudoelastic damping effect is not activated. In other words, if the amplitude is too small, the stress in the SMA is not enough to induce martensitic transformation, so no hysteretic damping occurs. In the simulations shown, hysteretic damping is active at smaller displacements in NiTi at 271 K (figure 9) than in CuZnAl (figure 11), which explains the lower amplitudes observed in figure 11.

However, the total damping capacity of the SMA, i.e., the total energy absorbed per loading cycle, is directly related to the stress hysteresis of the martensitic transformations considered. The hysteresis of the 18R–6R transformation is greater than the hysteresis of the NiTi alloys simulated, so the 18R–6R transformation has the potential to dissipate more energy per load cycle, if the amplitude of movement is high enough to induce the martensitic transition. As a consequence, a nonlinear relationship is established between the amplitude of excitation and the energy dissipated per cycle, which has a direct effect on the dynamic behavior of the system. A detailed analysis of this behavior will be published in future works.

From the results obtained in this study, we can see that the dynamic behavior of SMA-based damping systems is complex, nonlinear and several variables have a direct effect on the behavior of a mass–spring system with SMA damping.

Conclusions

A preliminary numerical model that is capable of simulating two consecutive martensitic transitions (β-18R and 18R–6R) in pseudoelastic Cu-base SMAs has been presented. The model was incorporated into a one degree of freedom mass–spring system so that the damping provided by the SMA can be assessed.

The introduction of SMA damping changes the dynamic response of the system. The SMA damper proposed in this manuscript is very efficient and its main effects are an increase in the rigidity and an important reduction in the maximum amplitude of the system.

The simulations have shown that, besides increasing the rigidity of the system, the SMA damper also dissipates energy, which makes it more efficient at reducing the dynamic response associated to external excitation than merely increasing the rigidity of the system.

Acknowledgments

The authors acknowledge financial support from pict 2012-0884 and UNCuyo, CONICET-Argentina, CNPq-Brasil and CAPES/PROEX-Brasil, through the Post-Graduate Program in Metallurgical, Materials and Mining Engineering at UFMG.

References

[1] DesRoches R, McCormick J and Delemont M 2004 *J. Struct. Eng.* **130** 38–46
[2] Saburi T 1998 *Shape Memory Materials* ed K Otsuka and C M Wayman (Cambridge, UK: Cambridge University Press) pp 49–96
[3] Yawny A, Sade M and Eggeler G 2005 *Z. Metallkd.* **96** 608–18
[4] Yawny A, Olbricht J, Sade M and Eggeler G 2008 *Mater. Sci. Eng.* A **481–2** 86–90
[5] Isalgue A, Torra V, Yawny A and Lovey F C 2008 *J. Therm. Anal. Calorim.* **91** 991–8
[6] Olbricht J, Yawny A, Condó A M, Lovey F C and Eggeler G 2008 *Mater. Sci. Eng.* A **481–2** 142–5
[7] Ahlers M 1986 *Prog. Mater. Sci.* **30** 135–86
[8] Tanaka Y, Himuro Y, Kainuma R, Sutou Y, Omori T and Ishida K 2010 *Science* **327** 1488–90
[9] Omori T, Ando K, Okano M, Xu X, Tanaka Y, Ohnuma I, Kainuma R and Ishida K 2011 *Science* **333** 68–71
[10] Krooss P, Niendorf T, Karaman I, Chumlyakov Y and Maier H J 2012 *Funct. Mater. Lett.* **4** 1250045
[11] Torra V, Isalgue A, Lovey F C and Sade M 2015 *J. Therm. Anal. Calorim.* **119** 1475–533
[12] Efstathiou C, Sehitoglu H, Kurath P, Folettib S and Davolib P 2007 *Scr. Mater.* **57** 409–12
[13] Efstathiou C, Sehitoglu H, Carroll J, Lambros J and Maier H J 2008 *Acta Mater.* **56** 3791–9
[14] Pelegrina J L and Ahlers M 1992 *Acta Metall. Mater.* **40** 3205–11
[15] Ahlers M and Pelegrina J L 1992 *Acta Metall. Mater.* **40** 3213–20
[16] Wollants P, Ross J R and Delaey L 1993 *Prog. Mater. Sci.* **37** 227–88
[17] Otsuka K and Wayman C M 1999 Mechanism of shape memory effect and superelasticity *Shape Memory Materials* ed K Otsuka and C M Wayman (Cambridge, UK: Cambridge University Press) pp 27–48
[18] Amireche R and Morin M 2009 A new stress-induced martensitic transformation in a Cu–Al–Be shape memory single crystal *Proc. Int. Conf. on Martensitic Transformations 2008, TMS* ed G B Olson *et al (Warrendale, USA)* pp 577–80
[19] de Castro Bubani F, Sade M and Lovey F 2012 *Mater. Sci. Eng.* A **543** 88–95
[20] Barceló G, Ahlers M and Rapacioli R 1979 *Z. Metallkd.* **70** 732–8
[21] Rao S *Mechanical Vibrations* 5th edn (Englewood Cliffs, NJ: Prentice-Hall) p 1084
[22] Mutter D and Nielaba P 2013 *J. Alloys Compd.* **577S** S83–7
[23] Zhou X and Li F 2014 *Comput. Mater. Sci.* **81** 530–7
[24] Mahnken R and Wilmanns S 2011 *Comput. Mater. Sci.* **50** 2535–48
[25] Gao X, Stebner A, Brown D W and Brinson L C 2011 *Acta Mater.* **59** 5924–37

[26] Rao A, Ruimi A and Srinivasa A R 2014 *Int. J. Solids Struct.* **51** 4554–71
[27] Li L J, Lei C H, Shu Y C and Li J Y 2011 *Acta Mater.* **59** 2648–55
[28] Soul H 2011 Aleaciones con memoria de forma, propiedades mecánicas y microestructura, Desarrollo de sistemas de amortiguamiento basados en el efecto superelástico *PhD Thesis (Engineering Sciences)* Bariloche, Universidad Nacional de Cuyo, Instituto Balseiro p 297
[29] Lovey F C, Rapacioli R and Chandrasekaran M 1981 *Phys. Status Solidi* a **68** K105–11
[30] Lovey F C, Torra V, Isalgué A, Roqueta D and Sade M 1994 *Acta Metall. Mater.* **42** 453–60
[31] Roqueta D, Lovey F C and Sade M 1997 *Scr. Mater.* **36** 385–91
[32] Roqueta D, Lovey F C and Sade M 1999 *Scr. Mater.* **40** 1359–65
[33] Newmark N M 1959 *J. Eng. Mech. Div.* **85** 67–94